

Improvement of the Adhesion Strength of MoSi₂-ZrB₂ Coating by Optimizing Particle Spraying and Subsequent Heat Treatment

Wang Lu, Fu Qian-gang, Liu Ning-kun, and Sun Jia

(Submitted November 17, 2015; in revised form September 5, 2016)

A MoSi₂-ZrB₂ coating was prepared on SiC-coated C/C composites by supersonic plasma spraying, and the effects of particle diameter and subsequent heat treatment in argon at different temperatures on the adhesion strength were studied. The results show that the MoSi₂-ZrB₂ coating sprayed with an average powder diameter of 29.2 μm could melt thoroughly and form a dense structure without micro-pore, which results in a relatively good adhesion strength of 11.4 MPa compared with 9.2 and 8.6 MPa of the coatings sprayed with the powder diameter of 58.2 and 35.5 μm. The coating presents a decreasing porosity from 2.2 to 1.5% and an increasing adhesion strength from 11.6 to 16.9 MPa after heat treatment at 800 °C, which is mainly caused by slight sintering of SiO₂ and B₂O₃.

Keywords coating, heat treatment, particle diameter, plasma spray

1. Introduction

Carbon/carbon (C/C) composites have attracted numerous attentions in decades, owing to their low density (<2.0 g/cm³), high strength and modulus, low coefficient of thermal expansion, good thermal impact resistance and stable mechanical properties at elevated temperature, which made them a logical choice as the thermal structural materials in the field of aeronautics and astronautics (Ref 1, 2). Unfortunately, these composites are easy to be oxidized above 400 °C in oxygen-containing environments. Coating is a feasible method to protect them against oxidation. Among ultrahigh-temperature ceramics, ZrB₂ and MoSi₂ are considered as the ideal candidate coating materials in thermal protective systems in aerospace applications, because of their excellent high-temperature mechanical properties, and good thermal shock and oxidation resistance between 700 and 1400 °C (Ref 3). Many techniques have been applied to fabricate the ZrB₂ or MoSi₂ based coatings, such as hot pressing (Ref 4), in situ reaction method (Ref 5, 6), and atmospheric plasma spraying (Ref 7-9).

Thermal spraying is a highly efficient method to deposit coating. However, the sprayed coatings exhibit a porous structure (Ref 10), which could not create an effective

barrier for substrate from corrosive environment. Many ways have been attempted to improve the coating homogeneity, release residual stress, reduce the porosity and enhance the adhesion strength, such as optimizing the spraying parameters (Ref 11, 12) and environment of spraying process (Ref 13-15), and performing a treatment of the coating to seal the holes (Ref 16).

In practical applications, the adhesion strength between coating and substrate directly influences the reliability of coatings. Numerous methods were proposed to evaluate the adhesion strength between the coating and substrate, i.e., indentation tests, shear tests and adhesion strength (Ref 17). The adhesion strength of plasma-sprayed coating lies on spraying system, spraying parameters, morphology of feed powder, roughness of substrate, residual stresses in coating and type of bond coating. Once the adhesion strength of the coating is not sufficient, the coating might be pulled out and loss protection ability (Ref 18). It is still a big challenge to improve the adhesion ability of the sprayed coatings.

Heat treatment is an effective and rapid technology to obtain a desirable sprayed coating. Ghadami (Ref 18) reported that some chemical reactions might happen between the coating materials and substrate after heat treatment above 900 °C and the adhesion strength presented an obvious improvement. Particle diameter is another significant parameter on the structure of coating, which has a direct relation with the melting degree of the particles and with the accumulation of lamellar droplets in the process of spraying. Berndt (Ref 19) reported that the adhesion strength of plasma-sprayed WC-Co coating could be improved with increasing melting degree of particle due to a better particle flattening. In addition, the bond coating could increase the adhesion strength of the resultant coating by reducing stresses in the coating. SiC coating prepared using pack cementation method shows dense structure, high combination strength with the substrate and rough surface. These performances are

Wang Lu, Fu Qian-gang, Liu Ning-kun, and Sun Jia, State Key Laboratory of Solidification Processing, Carbon/Carbon Composites Research Center, Northwestern Polytechnical University, Xi'an 710072, Shaanxi, People's Republic of China. Contact e-mails: wl2014@mail.nwpu.edu.cn and fuqiangang@nwpu.edu.cn.

beneficial for spraying the outer coating. Therefore, SiC coating is generally prepared on C/C composites to act as a bond coating.

In this work, a MoSi₂-ZrB₂ coating was prepared on SiC-coated C/C composites by supersonic plasma spraying. The effects of spraying particle diameter and heat-treatment temperature on the microstructures of MoSi₂-ZrB₂ coating were studied, and the interface de-bonding behavior between coating and substrate was also discussed.

2. Experimental

2.1 Coating Preparation

As the substrate, bulk 2.5D C/C composites were prepared via gradient chemical vapor infiltration method. Then they were cut into small cubes with a dimension of 10 × 10 × 10 mm and cylinders with a dimension of φ 25 × 5 mm, finally the specimens were cleaned with absolutely ethyl alcohol in the ultrasonic bath and dried at 80 °C for 2 h.

The inner SiC coating was prepared as a transition layer on 2.5D C/C specimens by pack cementation. Details about the preparation process were reported in (Ref 20). The outer MoSi₂-ZrB₂ coating was prepared by high-efficient supersonic plasma spraying (HEPJ-100, Armored Corps Engineering College, China). The feed powder of MoSi₂-ZrB₂ was prepared using centrifugal evaporation method (LGZ-5 centrifugal spray dryer, Wuxi Dongsheng spray drying machinery factory, China). MoSi₂ (mean diameter is 12.7 μm, 99% purity, Songshan tungsten and molybdenum materials Co. Ltd., China) and ZrB₂ (mean diameter is 13.5 μm, 99.99% purity, Dandong Chemical Co., Ltd., China) powders were dry-milled together in zirconium oxide pot for 2 h. First, polyvinyl alcohol (PVA) was dissolved into water with the concentration of 2 wt.% to obtain the solution. Then the same-mass solution and milled powders were mixed and evaporated at about 120 °C using centrifugal spray dryer.

The obtained powder was sieved by 200 and 400 grit meshes, and then the sieved powder was collected, respectively, and marked as follows: particle A (powder over 200 grit mesh), particle B (powder between 200 and 400 grit mesh), particle C (powder below 400 grit mesh). The coatings were prepared by supersonic plasma spraying with particles A, B, C, respectively. In order to obtain these coatings with the same thickness, the cross section of the sprayed coatings was observed under microscopy and the spray duration was adjusted accordingly. The spraying parameters were shown in Table 1. All of the spray parameters were the same for all the particle sizes. In order to observe the microstructure evolution of the spray particle, the sprayed particles were collected from the flame flow exit. They were directly sprayed into water, then the water vaporized at 80 °C, and the dry particles were obtained.

2.2 Heat Treatment of the Coated Samples

The MoSi₂-ZrB₂-coated samples sprayed with particle types A, B and C were placed in the furnace, filled with flowing argon and heated at a rate of 5 °C/min. The samples were heat-treated at 800, 1000 and 1200 °C, respectively, for 1 h, and then cooled inside the furnace to room temperature.

2.3 Characterization

Adhesion test was performed according to the standard test ASTM C633 (Ref 21), which was dedicated to thermal-sprayed coatings. The cylindrical SiC-coated C/C specimens were sprayed with 40MoSi₂-60ZrB₂ on one side. Then the cylindrical samples were joined both sides with two cylindrical counter parts using high-strength epoxy, which was solidified at room temperature for 24 h. The cylindrical counter parts have a dimension of φ 25 mm × 173 mm. The adhesion load was applied with a universal adhesion machine (CMT5304-30kN) on samples. The velocity of tensile is 5 mm/min. The largest force before failure, *F*, was recorded for each specimens. The strength value was averaged from three tests under the same condition and calculated according to Eq 1 (Ref 21).

$$\sigma = F/A(\text{MPa}) \quad (\text{Eq 1})$$

where σ is the adhesion strength value, *F* is the applied load, and *A* is the section area of sample.

The microstructure and fracture surface of the coatings were investigated by scanning electron microscope (SEM, JSM-6460, JEOL Ltd, Mitaka, Japan). The crystalline phases of as-sprayed and heat-treated coatings were identified using x-ray diffraction (XRD, X Pert PRO, PANalytical, Almelo, Netherlands). The particle diameter distribution and porosity of the coatings were measured using Image J software. First, at least five pictures of the sprayed coating microstructure were taken to get an even value. Then, binarization process of these pictures highlighted the pores, and the area of pores was calculated by the software. The SEM pictures of spray particles were taken to get the average particle diameter. The pictures were threshold into binary images, and then the image was scanned to find the edge of each particle. After statistical analysis by the software, the results of the particle count and average particle size were displayed.

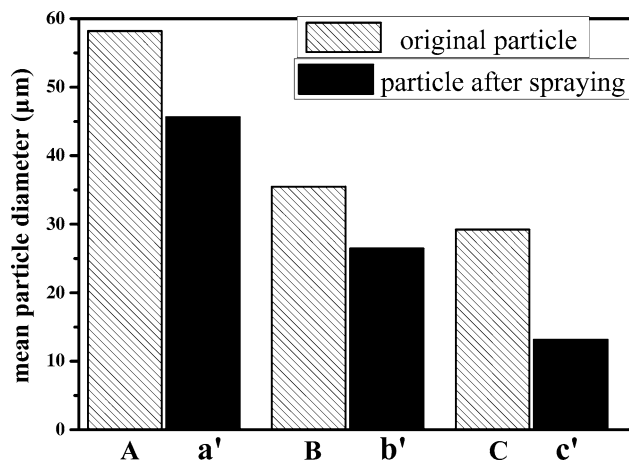
3. Results and Discussion

3.1 Effect of Particle Diameter

Figure 1 shows the mean diameter of three original particle types: A, B, C, and their corresponding particle after spraying: a', b', c'. The mean diameter of particles A, B, C decreases from 58.2 to 29.2 μm. The mean diameter of their corresponding particles, a', b', c' collected after spraying also decreases from 45.6 to 13.1 μm. It can be found that the particle diameter after spraying is smaller than that of the original one. Particle C has the

Table 1 Parameters of thermal spraying process

H ₂ (second gas)	Ar (primary gas)	Ar (carrier gas)	Power	Feed rate	Distance
4 L/min	75 L/min	10L/min	50 kW	20 g/min	100 mm

**Fig. 1** ZrB₂-MoSi₂ mean particle diameter of three types of powder before and after spraying

maximum reduction of diameter, reaching nearly half of originally average particle diameter. The volume shrinkage of the particle is mainly attributed to the high-temperature spray torch, which could melt the porous feed powder and then form a denser structure. The smaller particle has a bigger specific surface to absorb more heat for melting.

Figure 2 shows surface and cross-sectional morphologies of the original ZrB₂-MoSi₂ agglomeration powder and different diameters of sprayed powder. Figure 2(a-d) shows surface morphologies and Fig. 2(e-h) shows cross-sectional morphologies of particles. The particle of original powder contains thousands of little pieces, and these pieces cohered together to form a porous spherical structure (Fig. 2a) with a rough surface and a hole inside (Fig. 2e). After the process of spraying, some pieces were fused by the torch. From Fig. 2(b and f), it can be seen that only external thin layer of particle A was partly melt, which is still rough with obvious pieces. In addition, the particles were embedded at different horizontal planes in resin. Different particles would expose different positions when we polished the embedded samples. Therefore, the molten outer layer of particles could be observed. For particle B (Fig. 2c and g), they were mostly melted into a smooth surface and contain some un-melted part. As for particle C (Fig. 2d and h), they were totally melted, and have dense cross-sectional morphology without un-melted piece.

Figure 3 shows cross-sectional morphologies of SiC-coated C/C composites sprayed with particle type A (Fig. 3a), particle type B (Fig. 3b) and particle type C (Fig. 3c). The coating sprayed with particle types A, B and C has a thickness of ~84 µm. There are some cracks at the

interface between SiC and outer coating sprayed with particle A. Figure 3(b) shows that the coating is not dense with many pores in it. Figure 3(c) shows that the coating is dense without obvious pore. The formation reason of these structures could be explained as follows. In the process of spraying, particles impacted the substrate or deposited lamellar particles to form coating. Melting degree is a significant factor to determine the porosity of the coating. Melted part made the greatest degree of distortion to cater to the shape of the substrate and formed a dense structure (Fig. 3c). Whereas un-melted part has many pores in single particle, and the pores would distort to survive in the coating during deposition. Particle size is another important factor since spaces would form between flatten particles. The bigger the particle diameter, the greater the space is between them after flattening. Based on the above analyses, the coating sprayed with type C performed better property.

Figure 4 shows the adhesion strength of coatings sprayed with different diameters. Coating sprayed with particle C has the largest adhesion strength of 11.4 MPa. The coating sprayed with particle A has the weakest adhesion strength of 8.6 MPa. Particle C was fully melted during spraying, so all of them impacted the substrate to form a dense structure without un-melted part, which will alleviate the stress concentration around the un-melted part. This compact structure strengthened the interface between the substrate and the coating. Particles A and B could not melt fully, and stress concentration would be formed in their coatings around un-melted part and obvious gaps between droplets. Those resulting in a lower adhesion strength. From Fig. 3, the coating sprayed with particle C is denser than with particles A and B. The defects existed in coating were benefit for crack propagation and hence induced a weak adhesion strength of the coating.

Figure 5 shows the fracture surface morphologies of the coatings sprayed with different particle diameters after adhesion tests. Figure 5(a) presents a smoothly regular pit at the fracture surface of the outer coating, which was sprayed with particle A. The pit is the split-off mark of un-melted particle. From Fig. 5(b), the fracture surface of coating sprayed with particle B presents a lamellar structure. The fracture of coatings sprayed with particles A and B mainly occurs in the outer layer, because the surfaces were covered with large areas of outer coating. This inferring a weak cohesive adhesion strength of the outer coating. In Fig. 5(c), the most area of fracture surface was SiC inner coating which has been peeled off partially, and the rest outer coating is dense and jointed with SiC well. The fracture position indicates a strong cohesive adhesion strength of the outer coating. Figure 5(d) shows the macro-fracture graphs of the coating sprayed with

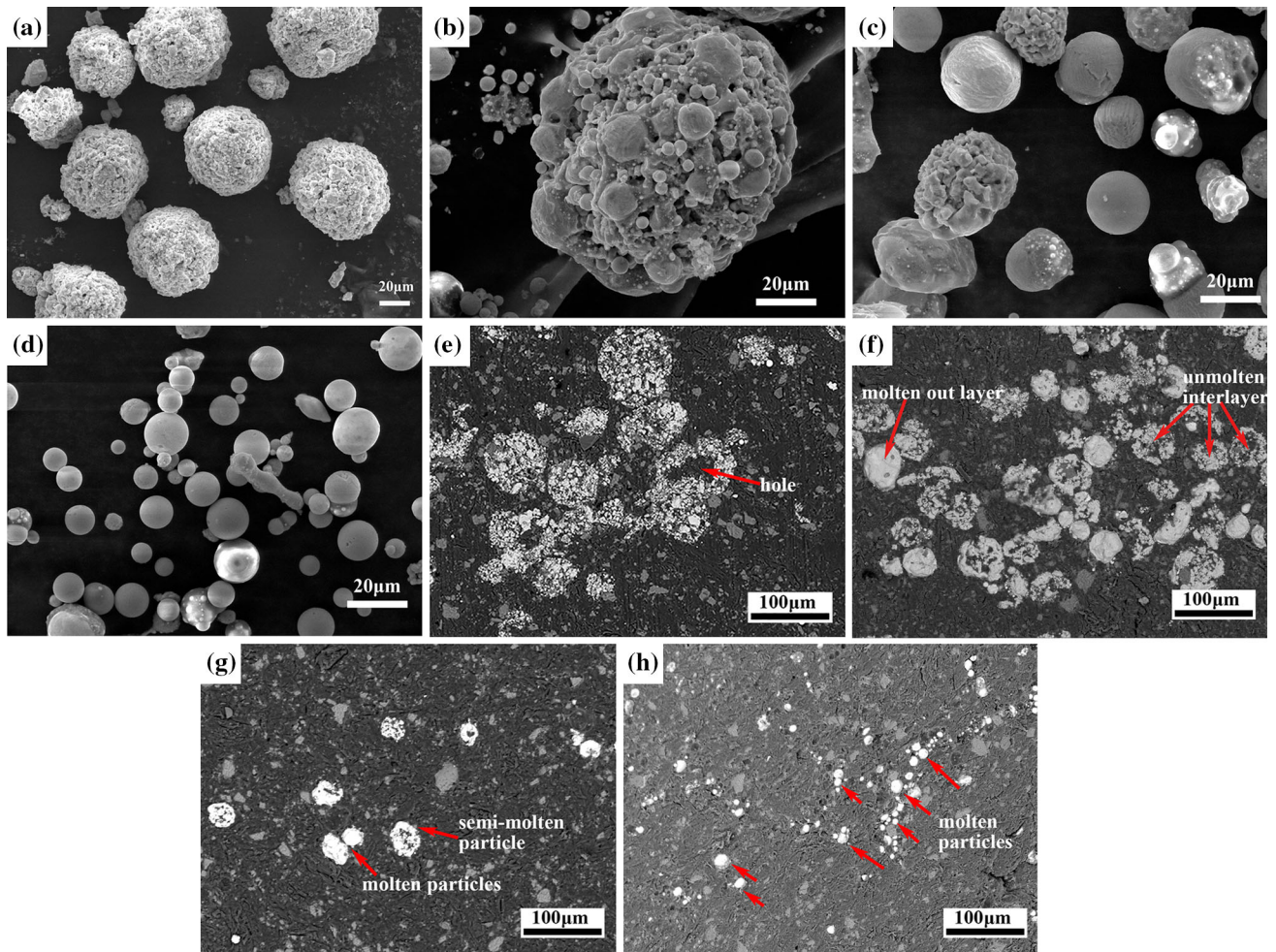
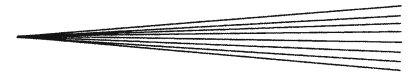


Fig. 2 Surface and cross-sectional morphologies of original agglomeration powder (a) (e) and different diameter of sprayed ZrB_2 - $MoSi_2$ powder particle type A corresponding to (b, f); particle type B corresponding to (c, g); particle type C corresponding to (d, h)

particles A, B and C. With the increasing of the particle diameter, the amount of peeled sprayed coating decreased. The fracture happened mainly at the interface between the sprayed outer coating and SiC coating.

3.2 Effect of Heat Treatment

Figure 6 shows the XRD patterns of each ZrB_2 - $MoSi_2$ coating before and after heat treatment for different temperatures. The as-sprayed ZrB_2 - $MoSi_2$ coating was composed of ZrB_2 , $MoSi_2$, monoclinic ZrO_2 , Mo_5Si_3 and SiO_2 . The plasma spraying process was carried out in air, and the original materials reacted with the oxygen to form new phases under high-temperature environment. ZrO_2 is the product of ZrB_2 and O_2 during spraying process. Mo_5Si_3 and SiO_2 is the product of $MoSi_2$ and O_2 . After heat-treated at 800 °C, the peak intensity of m- ZrO_2 phase became stronger. When the heat treatment temperature was 1000 °C, a new phase, tetragonal ZrO_2 , was detected due to the monoclinic-tetragonal transition of crystalline ZrO_2 at around 1000 °C, and the peak intensity of all phases increased. For heat treatment at 1200 °C, the peak

intensity became stronger, and the phase composition did not change compared with 1000 °C. The reason why the peak of Mo_3Si_5 and ZrO_2 become very strong after 1200 °C treatment should have two aspects. One is that the heat treatment will increase the crystal size of Mo_3Si_5 and ZrO_2 , and thus increase their crystalline. The other might be that oxygen still exists in the argon atmosphere which could react with $MoSi_2$ and ZrB_2 to form Mo_3Si_5 and ZrO_2 during heat treatment. No new alloy phase was formed during the heat treatment process.

Figure 7 shows the back-scatter scanning (BSE) cross-sectional microstructures of ZrB_2 - $MoSi_2$ coatings sprayed with particle B performed in the argon protecting environment for 1 h at 25 °C (Fig. 7a), 800 °C (Fig. 7b), 1000 °C (Fig. 7c) and 1200 °C (Fig. 7d). The as-sprayed coating (Fig. 7a) shows many interlayer pores and micro-cracks in it. After heat-treated at 800 °C, the coating became denser. With the further increase of the processing temperature, some obvious defects like pores and cracks were formed again in the coating. From Fig. 7(b), there are two phases in the coating, including the light gray phase marked as 1 and the dark gray phase marked as 2. From

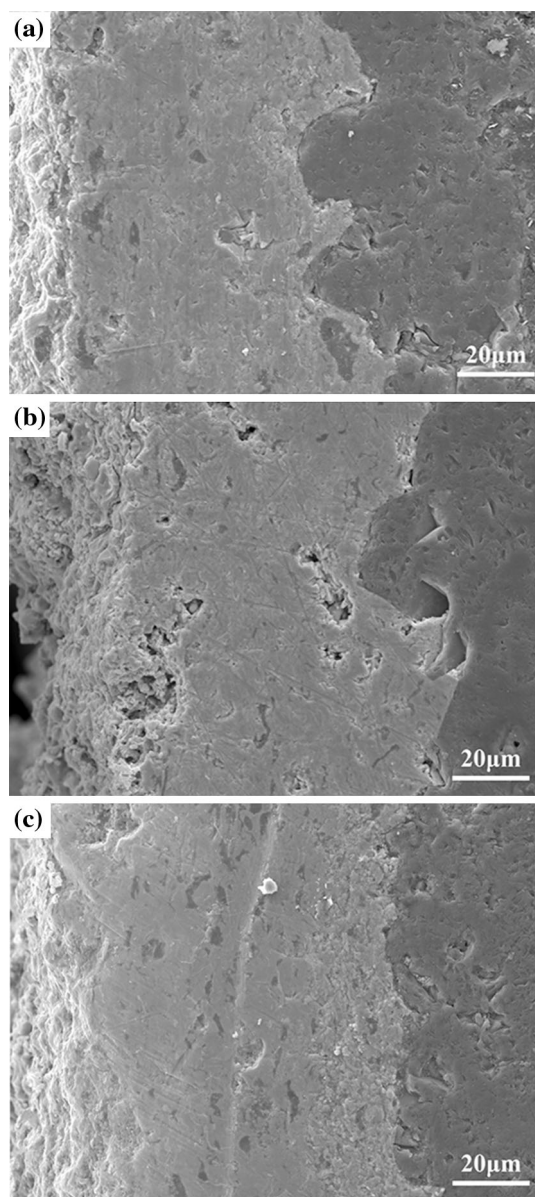


Fig. 3 Cross-sectional morphologies of coatings prepared on SiC-coated C/C composites with particle type A (a), particle type B (b) and particle type C (c)

the energy dispersive analysis results of phase 1 and 2, it can be seen that phase 1 consists of element O, Si, Mo with atomic number ratio of 35:26:30, and phase 2 consists of element O, B, Zr with atomic number ratio of 57:24:19. Combined these results with XRD in Fig. 6, it can be deduced that the phase 1 contains SiO_2 and MoO_3 , and phase 2 contains B_2O_3 and ZrO_2 in $\text{ZrB}_2\text{-MoSi}_2$ coating after heat treatment at 800°C . These phases were oxides of ZrB_2 and MoSi_2 during coating preparation. ZrB_2 oxidizes to form both ZrO_2 and B_2O_3 . The B_2O_3 is liquid above $\sim 425^\circ\text{C}$ but volatilizes above $\sim 1000^\circ\text{C}$ (Ref 22). SiO_2 and MoO_3 form as the oxidation product of MoSi_2 . The torch of spray has very high temperature to melt particles, then these particles were impacted on the cold

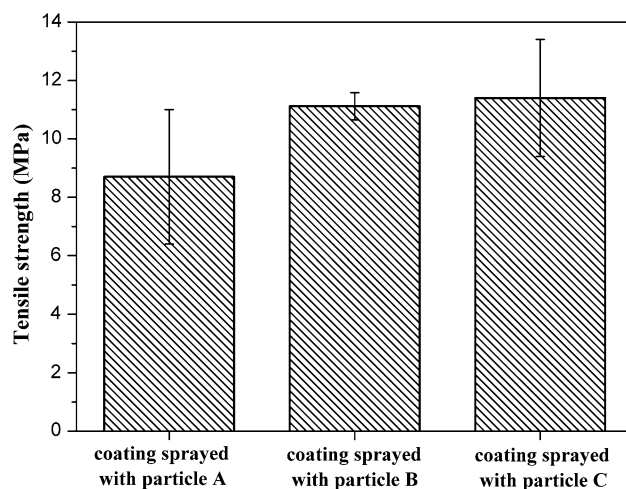


Fig. 4 Adhesion strengths of coatings sprayed with different diameter of $\text{ZrB}_2\text{-MoSi}_2$ powder

substrate to form coat in less than a second. This ultrafast speed and great temperature variation are essential conditions of glass formation. Hence, the MoO_3 and B_2O_3 could be hardly detected in the XRD. After heat-treated at 1200°C (Fig. 7d), the cross section of coating shows two regions, the left part contains few white phase and the right part still has some white phase, which confirms the evaporation of low melting phases.

Figure 8 shows the porosity of each $\text{ZrB}_2\text{-MoSi}_2$ coating after heat treatment for different temperatures. After heat-treated at 800°C , the porosity of $\text{ZrB}_2\text{-MoSi}_2$ coating decreased from 2.2 to 1.5%. With the increasing of the heat treatment temperature, the porosity of the coating increased to 3.0%. This porosity decreasing was mainly caused by the fusion of SiO_2 and B_2O_3 ($T_m = 445^\circ\text{C}$) (Ref 20) (the oxides of raw materials acquired in the process of spraying) at 800°C , which could flow to fill interlayer pores. Additionally, B_2O_3 benefits the fluidity of the SiO_2 at the intended temperature which facilitate the filling of cracks (Ref 23). When the temperature reached up to 1000°C , with the further increase of the processing temperature, low melting materials like MoO_3 (Ref 15) and B_2O_3 started to vapor, which could leave some pores. Additionally, during the heat treatment, ZrO_2 was partly transformed from monolithic phase into tetragonal phase, which leads to volume reduction and thus leaves pores in the coating.

Figure 9 shows the adhesion test result of $\text{ZrB}_2\text{-MoSi}_2$ coating sprayed with particles A, B and C after heat treatment for different temperatures. The adhesion strength of the coating sprayed with particle B increased from 11.6 to 16.9 MPa after heat-treated at 800°C , whereas it decreased with the increasing of the heat treatment temperature. Results indicated that a proper heat treatment temperature could optimize the microstructure of the coating and then increase the adhesion strength for the $\text{ZrB}_2\text{-MoSi}_2$ coating. The improved adhesion strength has a significant relationship with the fusion of SiO_2 and B_2O_3 , because they could

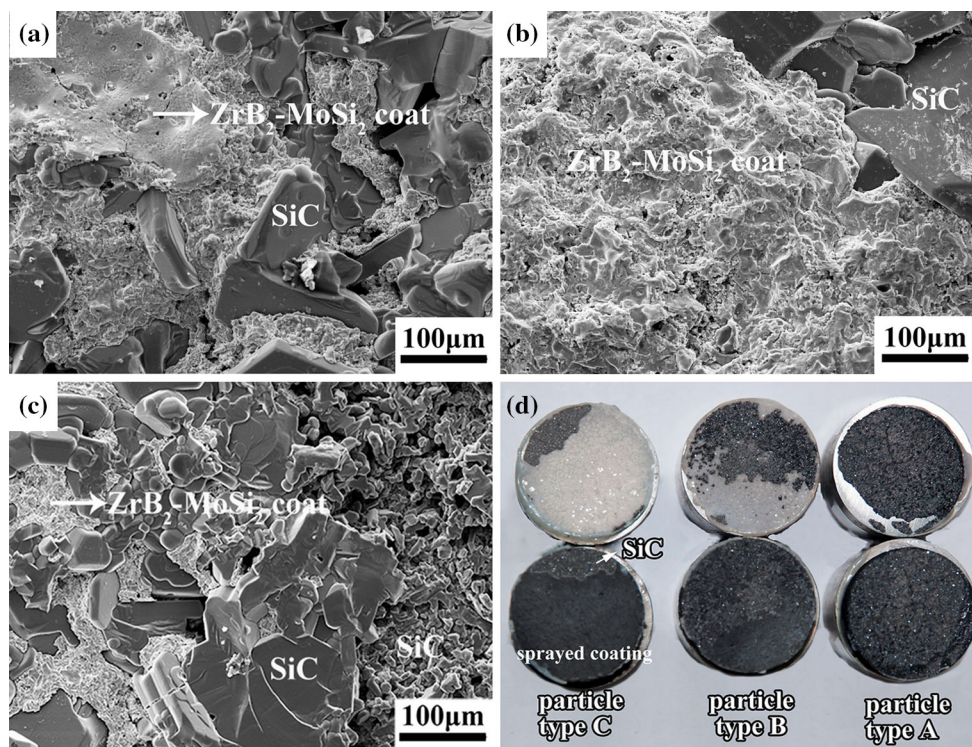


Fig. 5 Fracture surface morphologies of adhesion tests (a) coating sprayed with particle A, (b) coating sprayed with particle B, (c) coating sprayed with particle, (d) macro-fracture surfaces of the coating sprayed with particle types A, B and C

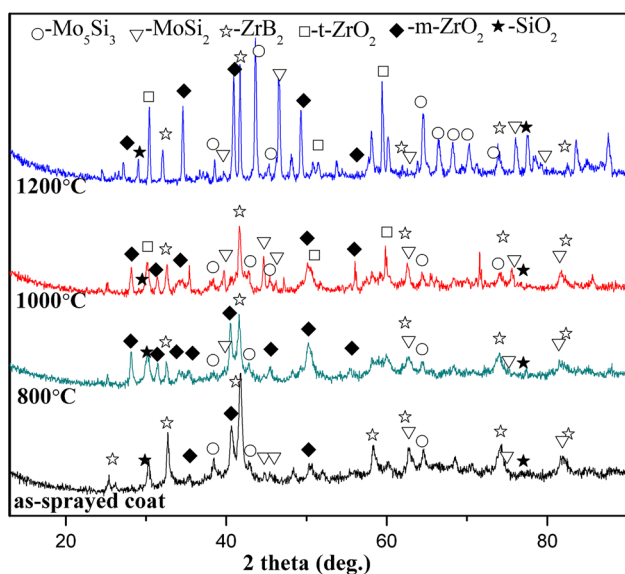


Fig. 6 XRD patterns of each ZrB_2 - $MoSi_2$ coating after heat treatment for different temperatures

make the coating denser and possess stronger cohesion ability. The adhesion strength of the coating sprayed with particle A has a slight decrease after heat treatment, and the heat treat temperature has little effect on the adhesion strength of the coating. The reason might be that the space of each droplet is too big to be filled with glass phases, and hence the strength is almost unchanged. The adhesion

strength of the coating sprayed with particle C increased after heat treatment at 800 °C and then decreased drastically at 1000 and 1200 °C. The reason should be that here still existed tiny spaces between these droplets, and the glass phases were easy to fill those spaces to form a denser structure of the coating at 800 °C. While the diameter of particle C is the smallest diameter, they have been totally melted to produce the most amount of glass phases during spraying process. This phenomenon is benefit for glass phases melting to fill the spaces; nevertheless, it is unfavorable for coating to be processed at above 1000 °C due to the evaporation of MoO_3 and B_2O_3 . The evaporation left a lot of pores in coating and eventually led to the decrease of the adhesion strength. Besides, during the deposition process, ZrO_2 formed as tetragonal phase was transformed into monolithic phase. After heat treatment, residual stress produced during deposition was reduced, which is also benefit for improvement of adhesion strength.

Figure 10 shows the fracture surfaces of the coatings for heat-treated at different temperatures after adhesion tests. The fracture surface in this work includes three kinds of components: C/C substrate (dark phase with parallel fiber bundles), SiC inner coating (dark gray crystalline phase) and ZrB_2 - $MoSi_2$ outer coating (light gray phase). Figure 10(a) shows a large area of ZrB_2 - $MoSi_2$ coating attached at the SiC coating, accompanied with pores and cracks between these two phases. The fracture happened between the outer ZrB_2 - $MoSi_2$ coating and inner SiC coating with an adhesion strength of 11.6 MPa. This

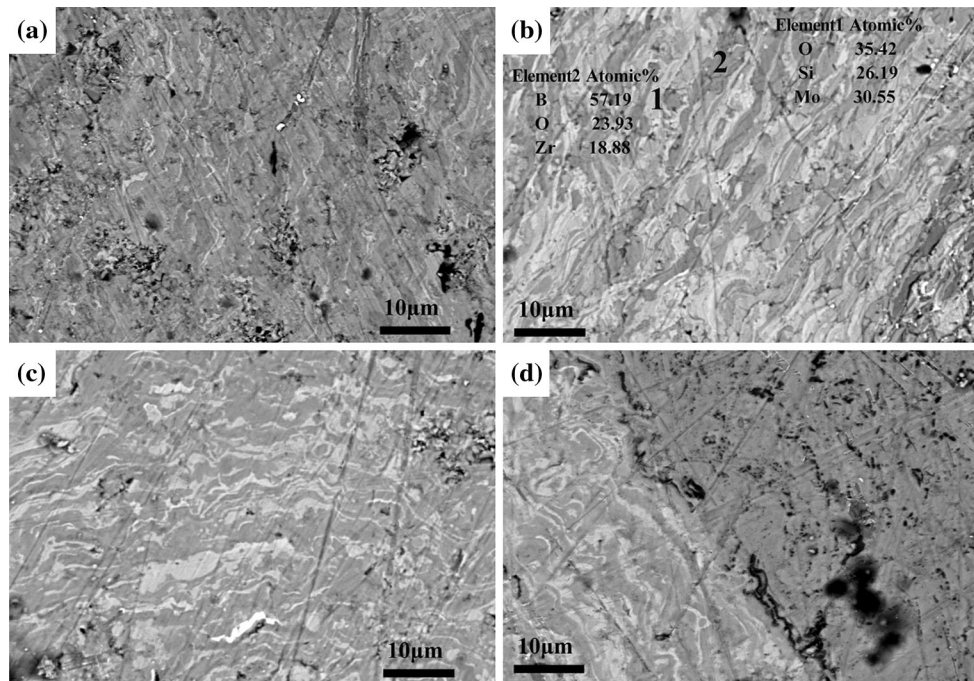


Fig. 7 BSE cross section images of ZrB_2 - $MoSi_2$ coatings sprayed with particle type B (a) as-sprayed, (b) heat-treated at 800 °C, (c) heat-treated at 1000 °C, (d) heat-treated at 1200 °C; and element dispersive analysis of phase 1 and phase 2 presents in (b)

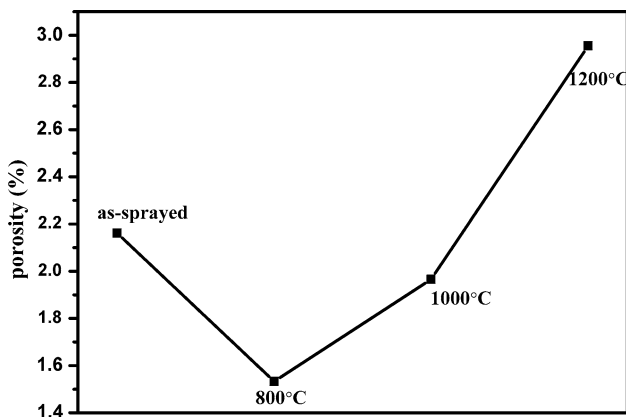


Fig. 8 Porosity of each ZrB_2 - $MoSi_2$ coating sprayed with particle type B after heat treatment for different temperatures

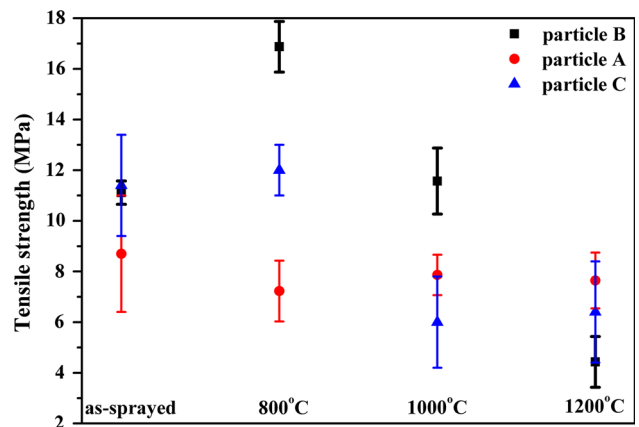


Fig. 9 Adhesion test result of each ZrB_2 - $MoSi_2$ coating sprayed with particles type A, B and C after heat treatment for different temperatures

demonstrated a weak adhesion strength of the outer coating with SiC coating, and a weaker cohesive strength of the outer coating itself. The weak adhesion strength was resulted from a mechanical joint of SiC and sprayed ZrB_2 - $MoSi_2$ coatings and a porous structure of the outer coating.

In Fig. 10(b), the fracture surface was composed of SiC coating, C/C substrate and basically no outer coating. It is obvious that the fracture mainly happened at the interface between SiC coating and C/C substrate, which indicates a stronger adhesion strength of SiC coating with C/C substrate than with ZrB_2 - $MoSi_2$ coating after being treated at 800 °C. This is attributed to the compact outer coating

after heat treatment. The defects in the outer coating like pores and cracks were healed by SiO_2 and B_2O_3 phases whose melting points were below 800 °C.

Figure 10(c, d) show the fracture surfaces of ZrB_2 - $MoSi_2$ coatings heat-treated at 1000 and 1200 °C. Their fracture happened within the outer coating, and it is clear that the outer coating was full of micro-pores. Additionally, the adhesion strengths of the coatings after heat-treated at 1000 and 1200 °C were obviously lower than that of the as-sprayed coating. This can be explained that MoO_3 and B_2O_3 (the oxides of the coating raw materials) began to evaporate at above 1000 °C, which produced micro-pores and micro-cracks in the outer coating and

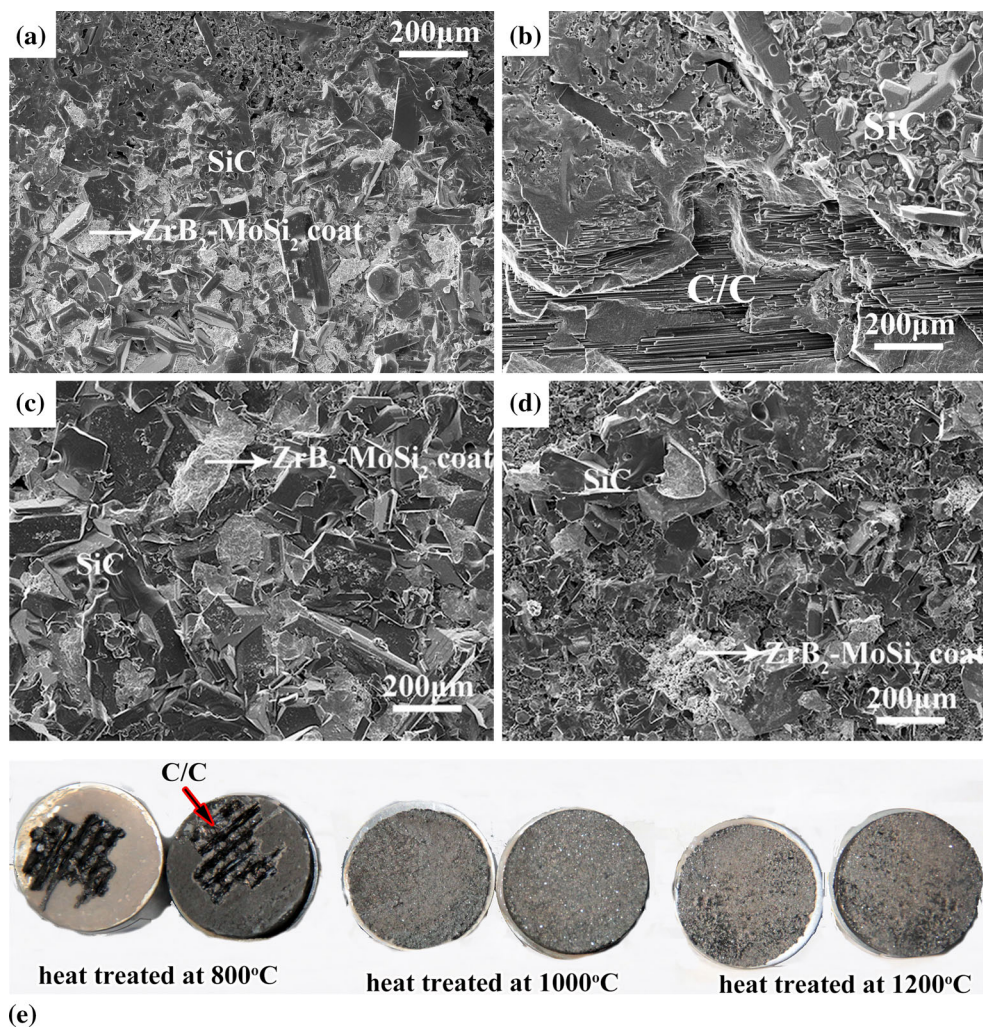


Fig. 10 Fracture surface morphologies of the coating sprayed with particle B after adhesion tests (a) as-sprayed, (b) heat-treated at 800 °C, (c) heat-treated at 1000 °C, (d) heat-treated at 1200 °C, (e) macro-fracture surfaces of the coating sprayed with particle type B after heat-treated at different temperature

finally resulted in a weak adhesion strength of the outer coating. Figure 10(e) shows macro-fracture surfaces of the coating sprayed with particle type B after heat-treated at 800, 1000 and 1200 °C. After 800 °C heat treatment, the fracture surface mainly formed in the C/C substrate. For 1000 °C, the fracture happened at the interface between SiC and the sprayed coatings. For 1200 °C, the fracture also happened in sprayed coatings, and lots of pores (black points) could be observed. Those pores correspond to the porous structure as shown in Fig. 7(d).

4. Conclusions

A MoSi₂-ZrB₂ coating was prepared on SiC-coated C/C composites by supersonic plasma spraying. The fine spraying particle with an average diameter of 29.2 μm could form a dense structure without micro-pore and alleviate the stress concentration around un-melted part,

which leads to a better adhesion strength of 11.4 MPa compared with 9.2 and 8.6 MPa of the coatings sprayed with the powder diameter of 58.2 and 35.5 μm.

Heat treatment of ZrB₂-MoSi₂ coating sprayed with particle diameter of 35.5 μm at 800 °C in argon atmosphere could reduce the porosity from 2.2 to 1.5%, enhance the homogenous of the coating and hence improve the adhesion strength of coating from 11.6 to 16.9 MPa, which might be ascribed to the formation of glass phases (SiO₂ and B₂O₃).

Acknowledgments

This work has been supported by 111 project (Grant No. B08040) and National Natural Science Foundation of China (Grant Nos. 51521061, 51572223 and 51272212), Project supported by the Research Fund of the State Key Laboratory of Solidification Processing (NWPU), China (Grant No. 142-TZ-2016).

References

1. N.S. Jacobson and D.M. Curry, Oxidation Microstructure Studies of Reinforced Carbon/Carbon, *Carbon*, 2006, **44**(7), p 1142-1150
2. Y.L. Zhang, F. Tian, W.Y. Zeng, B.X. Yang, H.J. Li, and K.Z. Li, Microstructure and Oxidation Behavior of C/C-ZrB₂-SiC Composites Coated with SiC Coating at High Temperature, *Corr. Sci.*, 2015, **100**, p 421-427
3. D. Sciti, M. Brach, and A. Bellosi, Oxidation Behavior of a Pressureless Sintered ZrB₂-MoSi₂ Ceramic Composite, *Mater. Res. Soc.*, 2005, **20**(4), p 922-930
4. J. Rodríguez-Sánchez, E. Sánchez-González, F. Guiberteau, and A.L. Ortiz, Contact-Mechanical Properties at Intermediate Temperatures of ZrB₂ Ultra-High-Temperature Ceramics Pressureless Sintered with Mo, Ta, or Zr Disilicides, *J. Eur. Ceram. Soc.*, 2015, **35**(11), p 3179-3185
5. X.R.X. Ren, H.J. Li, and Y.H. Chu, Preparation of Oxidation Protective ZrB₂-SiC Coating by In Situ Reaction Method on SiC-coated Carbon/Carbon Composites, *Surf. Coat. Technol.*, 2014, **247**, p 61-67
6. X.Y. Yao, H.J. Li, Y.L. Zhang, and Y.J. Zhang, Oxidation and Mechanical Properties of SiC/SiC-MoSi₂-ZrB₂ Coatings for Coating for Carbon/Carbon Composites, *J. Mater. Sci. Technol.*, 2014, **30**(2), p 123-127
7. J.Y. Mao, M. Liu, and J. Mao, Oxidation-resistance of ZrB₂-MoSi₂ Composite Coatings Prepared by Atmospheric Plasma Spraying, *J. Inorg. Mater.*, 2015, **39**(3), p 282-286
8. B.L. Zou, Y. Hui, and W.Z. Huang, Oxidation Protection of Carbon/Carbon Composites with a Plasma-Sprayed ZrB₂-SiC-Si/Yb₂SiO₅/LaMgAl₁₁O₁₉ Coating During Thermal Cycling, *J. Eur. Ceram. Soc.*, 2015, **35**(7), p 2017-2025
9. Y.L. Zhang, Z.X. Hu, B.X. Yang, J.C. Ren, and H.J. Li, Effect of Pre-oxidation on the Ablation Resistance of ZrB₂-SiC Coating for SiC-Coated Carbon/Carbon Composites, *Ceram. Int.*, 2015, **41**(2), p 2582-2589
10. L.F. Pierre, V.R. Joachim and I.B. Maher: *Thermal Spray Fundamentals*, 2013, p 943-944
11. Y. Bai, L. Zhao, Y.M. Qu, Q.Q. Fu, Y. Wang, K. Liu, J.J. Tang, B.Q. Li, and Z.H. Han, Particle In-Flight Behavior and its Influence on the Microstructure and Properties of Supersonic- Atmospheric- Plasma- Sprayed Nanostructured Thermal Barrier Coatings, *J. Alloy. Compd.*, 2015, **644**, p 873-882
12. K. Liu, J.J. Tang, Y. Bai, Q.Z. Yang, Y. Wang, Y.X. Kang, L. Zhao, P. Zhang, and Z.H. Han, Particle In-Flight Behavior and its Influence on the Microstructure and Mechanical Property of Plasma Sprayed La₂Ce₂O₇ Thermal Barrier Coatings, *Mater. Sci. Eng., A*, 2015, **625**, p 177-185
13. N. Prashant, G. Sivakumar, and K. Sudarshan, Solution Precursor Plasma Spray (SPPS) Technique of Catalyst Coating for Hydrogen Production in a Single Channel with Cavities Plate Type Methanol Based Microreformer, *Chem. Eng. J.*, 2015, **277**, p 168-175
14. B. Vautherin, M.P. Planche, and G. Montavon, Study of Metallic Powder Behavior in Very Low Pressure Plasma Spraying (VLPPS)—Application to the Manufacturing of Titanium-Aluminum Coatings, *Surf. Coat. Technol.*, 2015, **275**, p 341-348
15. F. Azarmi, Vacuum Plasma Spraying, *Adv. Mater. Process.*, 2005, **163**(8), p 37-39
16. S. Paul, A. Cipitria, I.O. Golosnoy, L. Xie, M.R. Dorfman and T.W. Clyne J, Effects of Impurity Content on the Sintering Characteristics of Plasma-Sprayed Zirconia, *Therm. Spray Technol.*, 2007, **16**(5-6), p 798-803
17. M. Hadad, G. Marot, P. Démarécaux, D. Chicot, J. Lesage, L. Rohr and S. Siegmann, Adhesion Tests for Thermal Spray Coatings: Correlation of Bond Strength and Interfacial Toughness, *Surf. Eng.*, 2007, **23**(3), p 279-283
18. F. Ghadami, M. Heydarzadeh Sohi, and S. Ghadami, Effect of Bond Coat and Post-heat Treatment on the Adhesion of Air Plasma Sprayed WC-Co Coatings, *Surf. Coat. Technol.*, 2015, **261**, p 289-294
19. C.C. Berndt, *The Adhesion of Flame and Plasma Sprayed Coatings*, Monash University (1980)
20. Q.G. Fu, H.J. Li, X.H. Shi, K.Z. Li and G.D. Sun, Silicon Carbide Coating to Protect Carbon/Carbon Composites Against Oxidation, *Script. Mater.*, 2005, **52**(9), p 923-927
21. Standard Test Method for Adhesion or Cohesion Strength of Thermal Spray Coatings, ASTM Standard C633-79, American Society for Testing and Materials, Philadelphia, PA, 1999
22. E. Eakins, D.D. Jayaseelan, and W.E. Lee, Towards Oxidation-Resistant ZrB₂-SiC Ultrahigh Temperature Ceramics, *Metall. Mater. Trans. A*, 2011, **42**(4), p 878-887
23. Z. Derelioglu, A.L. Carabat, G.M. Song, S. van der Zwaag, and W.G. Sloof, On the Use of B-alloyed MoSi₂ Particles a Crack Healing Agents in Ytria Stabilized Zirconia Thermal Barrier Coatings, *J. Eur. Ceram. Soc.*, 2015, **35**, p 4507-4511